Chemical Physics Letters 713 (2018) 272–276

Contents lists available at ScienceDirect

Chemical Physics Letters

journal homepage: www.elsevier.com/locate/cplett

Research paper

Effect of NiO impurity on the magneto-transport properties of the $La_{0.7}Ba_{0.3}MnO_3$ granular manganite

Abd El-Moez A. Mohamed*, Aml M. Mohamed, A. ElShafaie, H.F. Mohamed, A.K. Diab, A.M. Ahmed

Department of Physics, Faculty of Science, University of Sohag, Sohag 82524, Egypt

HIGHLIGHTS

- $La_{0.7}Ba_{0.3}MnO_3/x$NiO composites were prepared by solid state reaction method.
- NiO addition changes the transport properties of $La_{0.7}Ba_{0.3}MnO_3$ compound.
- The room temperature MR of $La_{0.7}Ba_{0.3}MnO_3$ is enhanced with NiO addition.
- The Curie temperature of $La_{0.7}Ba_{0.3}MnO_3$ is not affected too much with NiO addition.
- The thermoelectric properties of $La_{0.7}Ba_{0.3}MnO_3$ are changed with NiO addition.

ARTICLE INFO

Keywords:
A. Magnetic materials
B. Magnetic properties
D. Electrical properties
D. Thermoelectric properties

ABSTRACT

Magnetoresistive, magnetic and thermoelectric properties of the $La_{0.7}Ba_{0.3}MnO_3/x$NiO system are studied. The x-ray diffraction shows the coexistence of the NiO and the $La_{0.7}Ba_{0.3}MnO_3$ phases in doped composites, revealing their interaction lack. This suggests the precipitation of the NiO at grain boundaries and on the $La_{0.7}Ba_{0.3}MnO_3$ surface, interrupting the conduction between grains. Hindering the direct contact between the $La_{0.7}Ba_{0.3}MnO_3$ grains increases the resistivity and decreases the metal-semiconductor transition temperature, leading to the spin tunneling effect. This enhances the room temperature magnetoresistance of the $La_{0.7}Ba_{0.3}MnO_3$ compound from −11.25% to −42.7% and −17.24% for 5% and 20% of the NiO additive amount, respectively. The pristine $La_{0.7}Ba_{0.3}MnO_3$ compound shows a Curie temperature value of 348 K that fluctuates negligibly with the NiO addition. However, it decreases to 332 K at the x = 0.05 composite due to a tiny diffusion of NiO in the $La_{0.7}Ba_{0.3}MnO_3$ lattice at this composite. The thermoelectric power properties of the $La_{0.7}Ba_{0.}$3MnO3 compound are changed with the NiO addition. Where the hole conduction interval increases and the peak of the Seebeck coefficient is shifted towards higher temperatures.

1. Introduction

Perovskite doped manganites show outstanding phenomena such as the colossal magnetoresistance (CMR) and the magnetocaloric effect (MCE) [1,2]. The CMR plays an important role in potential magnetic applications such as magnetic sensors and information storage devices [3,4]. However, the practical implementation of the CMR is limited due to the required high magnetic fields. On the other hand, granular materials show a good magnetoresistive response at low magnetic fields that is known as the low field MR (LFMR) [5]. This effect is attributed to the spin-dependent tunneling process and carriers scattering across grain boundaries (GBs) [3,6]. Several studies have discussed the GBs role in the LFMR promotion. For example, Evetts et al. explained the boundaries polarization by the adjacent grains [7], and Guinea F proposed the tunneling process during the paramagnetic impurities at the GBs barriers [8]. This increased the interest in GBs physics and their modification by increasing system granularity. One of possible ways is introducing secondary phases with the ferromagnetic material. The secondary phase does not interact intrinsically with the ferromagnetic material, and instead it precipitates extrinsically between the ferromagnetic grains. It can be said that the secondary phase works as an artificial barrier against carriers conduction, leading to carriers tunneling that induces the LFMR effect.

The granular *manganite/secondary phase* systems have been investigated previously in several works as $La_{0.7}Sr_{0.3}MnO_3/Zr_2O_3$ [9], $La_{0.67}Ca_{0.33}MnO_3/SrTiO_3$ [10] and $La_{0.7}Ca_{0.3}MnO_3/BaTiO_3$ [11]. All

* Corresponding author.
E-mail address: abdmoez_hussien@science.sohag.edu.eg (A.E.-M.A. Mohamed).

https://doi.org/10.1016/j.cplett.2018.10.040
Received 18 September 2018; Received in revised form 8 October 2018; Accepted 16 October 2018
Available online 17 October 2018

reported results showed an enhancement in the magnetoresistive properties with the secondary phase addition. In this work, we are trying to make use of the spin-polarization tunneling process to enhance the magnetoresistive properties of the $La_{0.7}Ba_{0.3}MnO_3$ compound by introducing the NiO as a secondary phase in different ratios. It is worth mentioning that the $La_{0.7}Ba_{0.3}MnO_3$ compound is chosen in this study because it shows a magnetic transition close to room temperature, in contrast with some other compounds such as the $La_{0.7}Sr_{0.3}MnO_3$ and the $La_{0.7}Ca_{0.3}MnO_3$ that show magnetic transition far away above and below room temperature, respectively.

2. Experimental

The $La_{0.7}Ba_{0.3}MnO_3$ (LBMO) compound was prepared via the solid-state reaction method as reported in [9]. The LBMO/*x*NiO (mass ratio) composites with x = 0, 0.05, 0.15 and 0.2 were prepared by mixing stoichiometric amounts of the LBMO and the NiO. The mixture was pressed and heat treated at 1000 °C for 24 h. The electrical resistivity was measured at B = 0 T and B = 0.6 T magnetic flux density using the Van der Pauw technique. The MR was calculated from the formula $MR = (\rho_H - \rho_0)/\rho_0$, ρ_0 and ρ_H are resistivities at zero and 0.6 T applied magnetic flux density. The crystal structure was examined at room temperature by the x-ray diffraction (XRD) technique using a Bruker (Axs-D & Advance) powder diffractometer with Cu-Ka radiation (wavelength λ = 1.5406 A). The XRD patterns were refined with the Rietveld method using the FULLPROF program. The microstructure investigation was performed by the scanning electron microscope (SEM) technique and the energy dispersive x-ray analysis (EDX) is provided too, using a deposited gold layer (Au) during imaging process of the x = 0.15 sample. The temperature dependence of magnetization was carried out at H = 100 Oe applied magnetic field in the field cooling-field heating mode using a vibrating sample magnetometer (VSM). The thermoelectric measurements were performed using special machine design of two copper electrodes (upper and lower) sandwiching the disc sample with a thermal controlled gradient inside a vacuum chamber, and the signal from these electrodes are taken to a keithley.

3. Results and discussion

3.1. Structure

The XRD patterns in Fig. 1a show the high purity phase of the LBMO compound with additional NiO peaks in the doped composites. The peak positions and reflections are in agreement with [12]. The coexistence of both phases suggests the NiO precipitation at the boundaries and on the surfaces of the LBMO grains as seen in the SEM micrographs in Fig. 2, and the corresponding EDX spectra prove elements presence. The LBMO/xNiO system shows a stability in structural properties, where the R-3c rhombohedral structure characterizes all composites without a notable change in the cell volume (V) (see Table 1), and the corresponding Rietveld refinement profile of the LBMO compound is provided in Fig. 1b, the refinements accuracy (χ^2) are listed in Table 1. The stability in structural properties refers to the separated NiO and the LBMO phases. However, the observed fluctuation in Table 1 may refer to a tiny diffusion of the NiO in the LBMO lattice (in some composites as a partial substitution of Mn by Ni ions). It is worth mentioning the negligible change in the SEM grain size excludes its role in the magneto-transport properties change.

3.2. Electrical properties

The temperature dependence of dc electrical resistivity, ρ(T), is displayed in Fig. 3. The LBMO compound shows a metal-semiconductor resistivity transition temperature (T_{ms}) at 270 K due to the double exchange (DE) interaction [13]. NiO addition increases the LBMO resistivity and decreases the T_{ms} (see Table 2), however, a resistivity drop is observed at the x = 0.2 composite in agreement with [9,14]. Due to the NiO-LBMO interaction lack, the change in the LBMO transport properties with the NiO addition seems likely arising from extrinsic factors as the GBs effect. However, the suggested diffused tiny portion of NiO in the LBMO lattice may promote the resistivity with a small intrinsic component in some composites. To understand the intrinsic/extrinsic factors role in the transport properties of the LBMO/xNiO system let us propose that the conduction in the LBMO compound occurs through the direct contact between grains [15]. The segregated NiO increases the GBs resistance increases carriers scattering and interrupts the direct contact between grains, leading to the resistivity increase [16]. The increase in GBs resistance with the NiO addition can be realized through the systematic increase in the low-temperature resistivity (at 90 K) (see Fig. 3), which is a temperature independent component arises mainly from the GBs effect. It is worth mentioning that the resistivity drop at the x = 0.2 composite is in agreement with [9,14] and can be attributed to the agglomeration of the NiO away from the GBs that leads to a smaller GBs thickness and resistance [13].

The ρ(T) data were analyzed above the T_{ms} with the well-established small polaron hopping (SPH) and the variable range hopping (VRH) models. These models work in two different temperature ranges. The SPH model with the $\rho/T = \rho_0\ exp(E_\rho/k_BT)$ formula [17] fits the

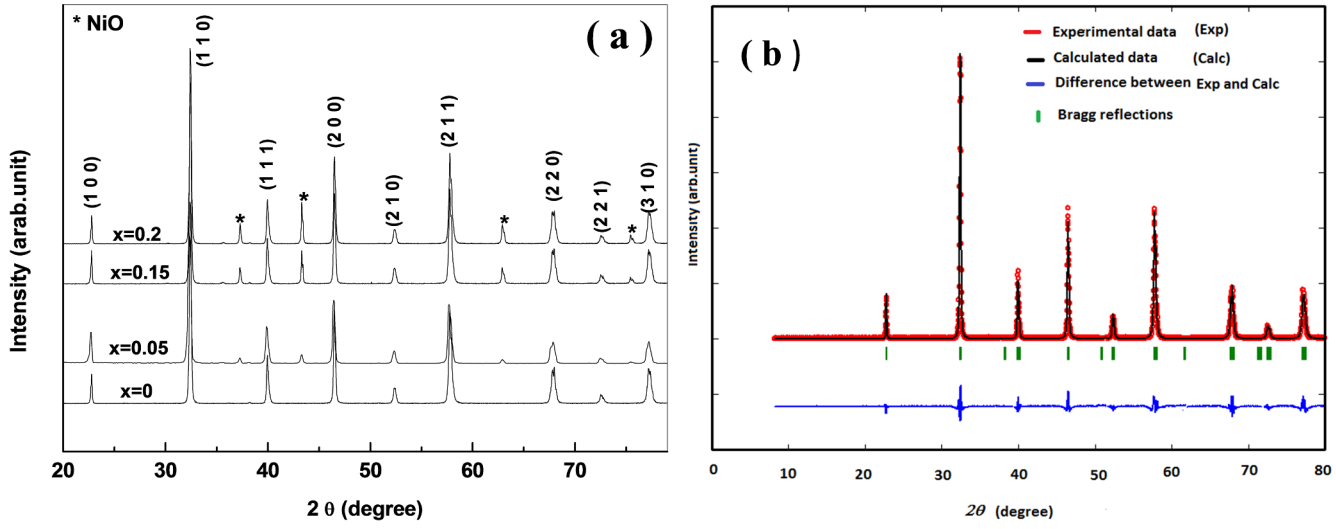

Fig. 1. (a) XRD patterns of the LBMO/xNiO composites and (b) Rietveld refinement profile of the LBMO compound.

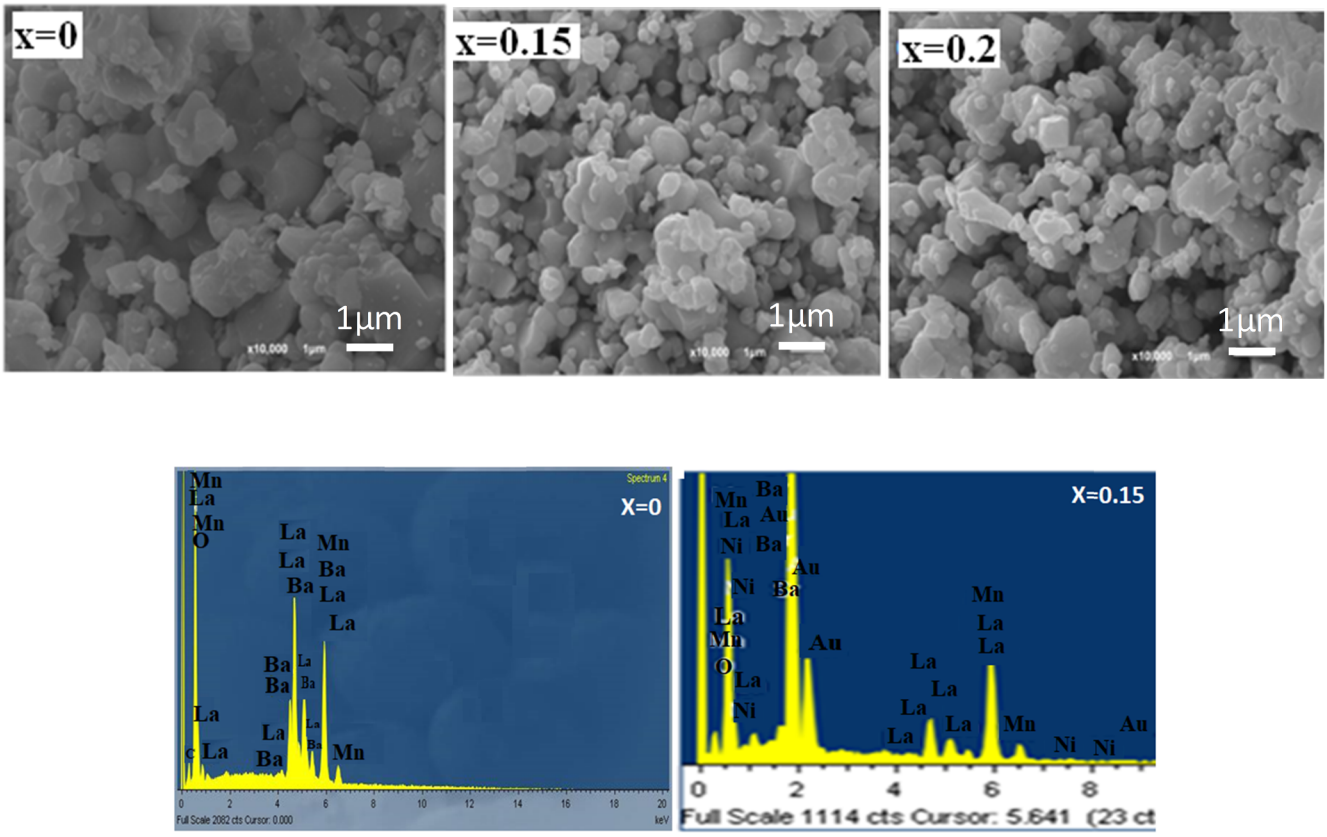

Fig. 2. SEM micrographs and EDX spectra of the LBMO/*x*NiO composites.

Table 1
Lattice parameters (a and c), cell volume (V), SEM grain size (G) and the goodness of fitting for Rietveld refinement (χ^2) for the $La_{0.7}Ba_{0.3}MnO_3/xNiO$ system.

x	a (Å)	c (Å)	V (Å)	G (μm)	χ^2
0	5.529	13.483	356.98	0.96	1.62
0.05	5.527	13.351	355.21	–	2.11
0.15	5.529	13.483	356.98	0.989	2.5
0.2	5.527	13.351	356.31	0.849	2.3

experimental resistivity data at $T > \theta_D/2$ as seen in Fig. 4a (ρ_0 is a constant, E_ρ is the activation energy, k_B is the Boltzmann constant, θ_D is the Debye temperature and $\theta_D/2$ is the deviation temperature from the linearity of this model). E_ρ increases monotonically with the increase in NiO content up to x = 0.15 (see Table 2). This is because NiO works as a scattering center, localizing the e_g electron. The drop in the E_ρ value at the x = 0.2 composite refers to the smaller e_g electron localization due to the smaller NiO effect on the GBs at this composite. Table 2 also shows the decrease in θ_D and phonon frequency (υ_{ph}) values of the LBMO compound with the NiO addition (υ_{ph} was determined from the $h\upsilon_{ph} = k_B\theta_D$ formula). On the other hand, the VRH model with the $\sigma = \sigma_0 exp\ (T_0/T)^{-1/4}$ formula [17] is applicable at $T_{ms} < T < \theta_D/2$ temperature range (see Fig. 4b), T_0 is the Mott characteristic temperature = $18/k_B N(E_f)a^3$, $N(E_f)$ is the density of states near the Fermi level and $1/a$ is the localization length ($a = 2.22\,nm^{-1}$) [18]. $N(E_f)$ decreases with the NiO addition up to x = 0.15 and increases for the x = 0.2 composite that is in agreement with the resistivity measurements, and this may refer to carriers scattering and e_g electron localization.

The temperature dependent MR in Fig. 5 shows the continuous decrease in the MR of the LBMO compound with temperature elevation, passing through a small peak around the T_{ms} with a maximum value of

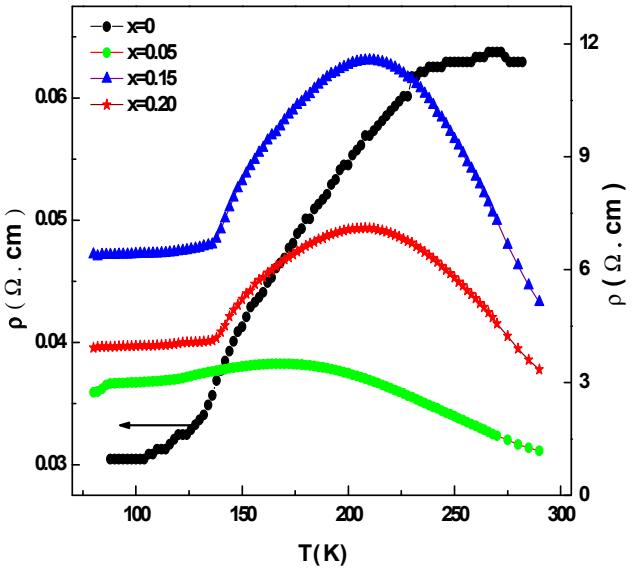

Fig. 3. Temperature dependent resistivity curves in zero magnetic field for the LBMO/xNiO system.

15%. In doped composites, the MR shows an obvious plunge around 140 K then passes through a wide hump, in agreement with the reported results in [9,11], except the x = 0.05 composite that shows a linear increase in the MR after the plunge. It is clear from Fig. 5 that the x = 0.2 composite shows MR values greater than the LBMO compound over the whole temperature range (except at the plunge), in contrast with the x = 0.15 composite that shows a smaller MR. x = 0.05 and x = 0.2 composites are considered as the best conditions, where they show a room temperature MR values of −42.71% and −17.24%,

Table 2
T_{ms} (K), T_c (K), SPH and VRH parameters for the LBMO/xNiO system.

X	T_{ms} (K)	T_c (K)	E_ρ (mev)	E_s (mev)	θ_D (K)	υ_{ph} (Hz)	$N(E_f)$ eV^{-1} cm^{-3}	R_h (Å)	E_h (mev)
0	270	348	*50.86*	*3.19*	*572*	*1.19 × 10¹³*	6.12×10^{24}	17.8	66
0.05	168	332	*126.46*	*5.23*	*507*	*1.05 × 10¹³*	8.30×10^{20}	10.3	38
0.15	210	351	*136.32*	*7.35*	*516*	*1.07 × 10¹³*	7.51×10^{20}	16	59
0.2	208	346	*128.44*	–	*524*	*1.09 × 10¹³*	11.4×10^{21}	14.7	54

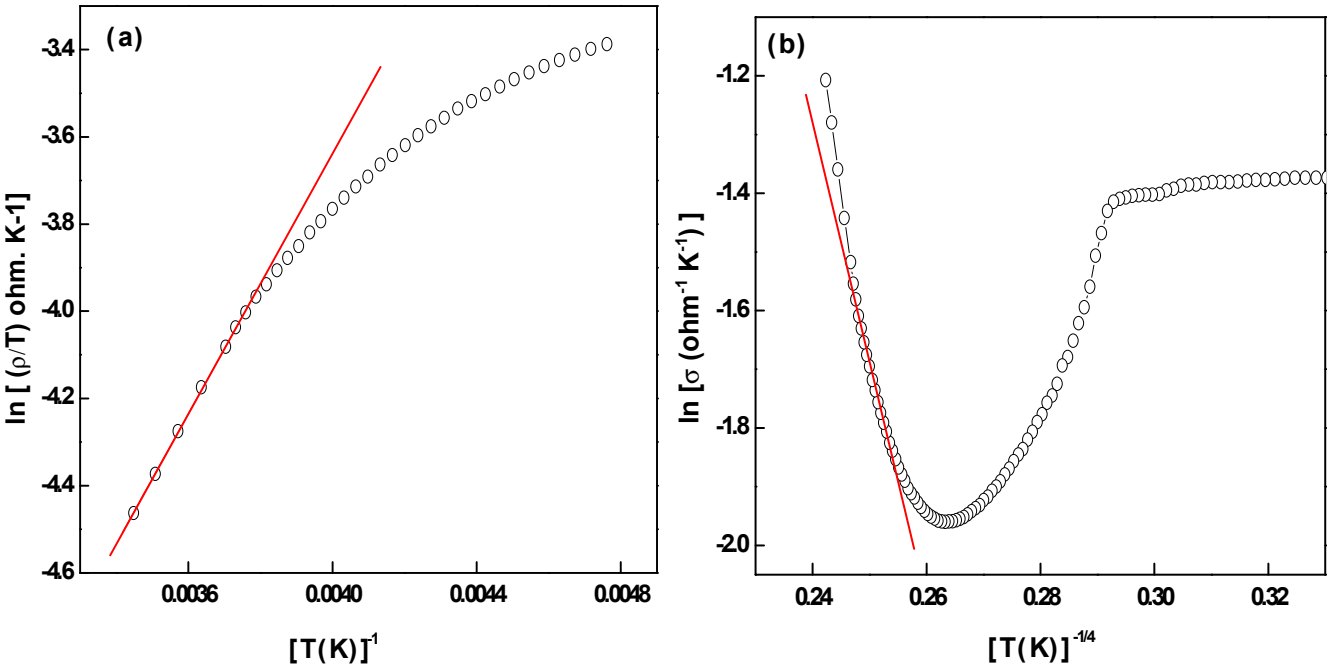

Fig. 4. The resistivity data fitting with (a) SPH and (b) VRH models, for the LBMO/$NiO_{0.2}$ composite.

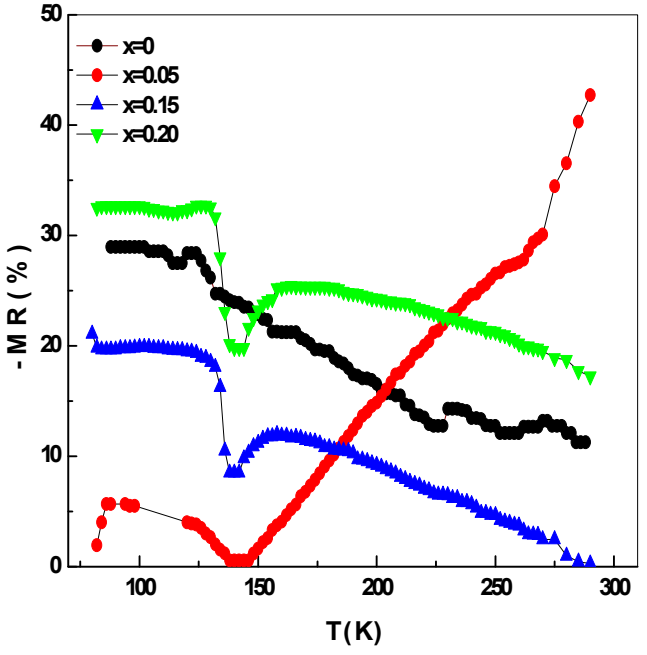

Fig. 5. Thermal variation of MR for the LBMO/xNiOsystem.

respectively, which are greater than the pristine LBMO (−11.25%). This enhancement in MR with NiO addition refers to the spin-dependent tunneling effect between grains as a result of the increase in GBs thickness [6,19].

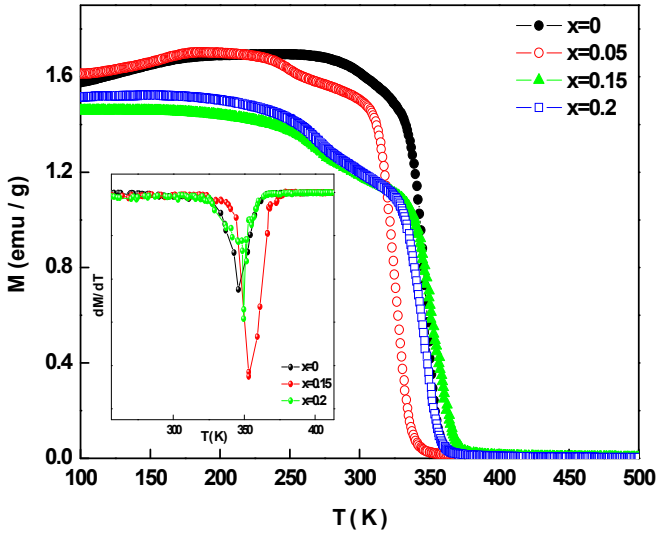

Fig. 6. Temperature dependence of magnetization for the LBMO/NiO system at H = 100 Oe, and the inset shows the dM/dT curves.

3.3. Magnetization

The temperature dependence of dc magnetization M(T) in Fig. 6 shows the ferromagnetic-paramagnetic (FM-PM) transition for all composites at the Curie temperature (T_c). The T_c value was determined according to the minimum of the M(T) derivative curves (dM/dT) as displayed in the inset of Fig. 6. The pristine LBMO compound shows a

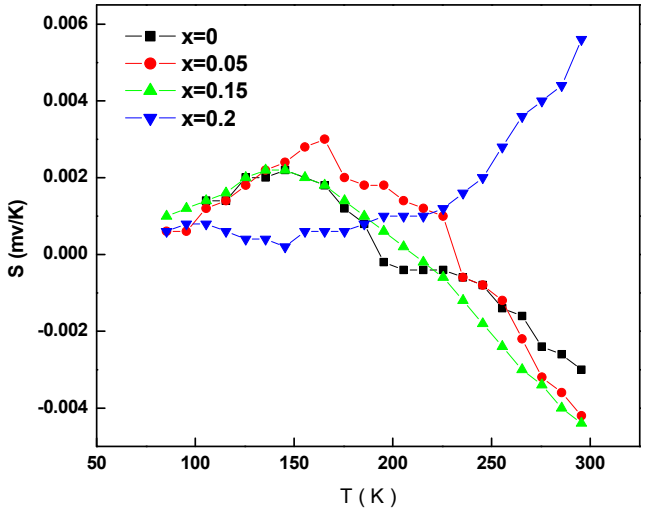

Fig. 7. The temperature dependence of Seebeck coefficient for the LBMO/xNiO system.

T_c value of 348 K, which is slightly preserved (~ ± 3K) with the NiO addition, except the x = 0.05 composite that shows a lower value of 332 K. This large decrease in the T_c value at this composite may refer to the antiferromagnetic Mn−O−Ni bonds formation due to the dissolved Ni^{2+} ions in the LBMO lattice that interrupt the ferromagnetic ordering. The magnetization of the LBMO compound decreases with the NiO addition due to the decrease in the ferromagnetic LBMO ratio and the increase in the antiferromagnetic NiO ratio. Moreover, the observed knee in the doped composites is attributed to the impurity presence and the ferromagnetic ordering interruption [19,20]. It is worth mentioning that the observed difference between the T_{ms} and the T_c values was reported and attributed to their different origin [21]. Where the T_c is an intrinsic property depends on the internal ferromagnetism of the grain that is preserved without any change due to the interaction lack, meanwhile, the T_{ms} is an extrinsic property that is affected by the GBs presence.

3.4. Thermoelectric power (TEP)

Fig. 7 presents the temperature dependence of Seebeck coefficient, S (T), for all composites. The pristine LBMO compound shows a maximum value of Seebeck coefficient (S_m) at temperature T_s = 145 K. It also exhibits a crossover from positive to negative S sign at temperature T^* = 192 K, meaning the dominance of hole conduction below this temperature. The hole conduction interval for the LBMO compound increases from 192 K to 230 K, 220 K with increasing the NiO content to 5%, 15% and vanishes for further amounts. The NiO addition increases the S_m value with a shift towards higher temperatures. The change in **S** sign from positive to negative at low temperatures suggests a change in the electronic state. In more details, the e_g band becomes degenerate at low temperatures showing the positive S sign. However, this degeneracy increases with temperature elevation, changing the S sign [22]. On the other hand, the negative S sign at high temperatures refers to the high mobility of electrons in the e_g conduction band. It is worth mentioning the increase in the absolute value of x = 0.2 refers to the strong correlation of 3d electrons and the characteristic spin degeneracy [23]. The high-temperature TEP data were fitted with the Mott equation $S = k_B/e(E_s/k_BT + \alpha)$ [17], E_s is the TEP activation energy and α is a constant. As seen in Table 2, the E_s value of the LBMO compound increases monotonically with the NiO addition, this is due to the increase in carriers scattering as a result of the NiO clustering at GBs.

4. Conclusion

Magneto-transport properties of the $La_{0.7}Ba_{0.3}MnO_3/x$NiO composites are studied. The R-3c rhombohedral symmetry characterizes all composites revealing structure stability with the NiO addition. NiO addition changes the transport properties of the pristine $La_{0.7}Ba_{0.3}MnO_3$ manganite compound, where it increases the resistivity and shifts the T_{ms} towards lower temperatures. The change in transport properties is due to the increase in grain boundaries resistance, which enhances the magnetoresistive properties through the spin tunneling effect. For example, the room temperature magnetoresistance of the $La_{0.7}Ba_{0.3}MnO_3$ compound is enhanced from −11.25% to −42.71% and −17.24% for x = 0.05 and x = 0.2 composites, respectively. The magnetic measurements show the negligible change in the T_c value for the $La_{0.7}Ba_{0.3}MnO_3$ compound with the NiO addition due to the interaction lack. The thermoelectric power measurements show a monotonic increase in the thermal activation energy and an enhancement in the hole interval conduction with the NiO addition.

Acknowledgement

This work was finically supported by the Science and Technology Development Fund (STDF), Egypt, Grant Project No. 3002.

References

[1] T. Zhang, X.P. Wang, Q.F. Fang, X.G. Li, Magnetic and charge ordering innanosized manganites, Appl. Phys. Rev. 1 (2014) 031302.
[2] M. Khelifi, R. M'nassri, A. Selmi, H. Rahmouni, K. Khirouni, N. Chnib Boudjada, A. Cheikhrouhou, J. Magn. Magn. Mater. 423 (2017) 20–26.
[3] H.L. Ju, J. Gopalakrishnan, J.L. Peng, Q. Li, G.C. Xiong, R.L. Greene, Phys. Rev. B 5 (1995) 16143(R).
[4] R. Jemai, R. M'nassri, A. Selmi, H. Rahmouni, K. Khirouni, N. Chniba Boudjada, A. Cheikhrouhou, J. Alloy Compds 693 (2017) 631–641.
[5] H.Y. Hwang, S.W. Cheong, N.P. Ong, B. Batlogg, Phys. Rev. Lett. 77 (1996) 2041.
[6] A. Gupta, J.Z. Sun, J. Magn. Magn. Mater. 200 (1999) 24.
[7] J.E. Evetts, M.G. Blamire, N.D. Mathur, S.P. Isaac, B.S. Teo, L.F. Cohen, J.L.M. Driscoll, Philos. Trans. R. Soc. London Ser. A 356 (1998) 1593.
[8] F. Guinea, Phys. Rev. B 58 (1998) 9212.
[9] A.M. Ahmed, H.F. Mohamed, A.K. Diab, A.A. Mohamed, A.E.A. Mazen, A.M. Mohamed, Indian J. Phys. 89 (2015) 561.
[10] D.K. Petrov, L.K. Eibaum, J.Z. Sun, C. Feild, P.R. Duncombe, Appl. Phys. Lett. 75 (1999) 995.
[11] Q. Jiang, J. Yang, C. Nan, Ferroelectrics 489 (2015) 60–64.
[12] J. Ardashti Saleh, I. Abdolhosseini Sarsari, P. Kameli, H. Salamati, J. Magn. Magn. Mater 465 (2018) 339.
[13] N. Kallel, G. Dezanneau, J. Dhahri, M. Oumezzine, H. Vincent, J. Magn. Magn. Mater. 261 (2003) 56.
[14] L.W. Lei, Z.Y. Fu, J.Y. Zhang, H. Wang, Mater. Sci. Eng. B 128 (2006) 70.
[15] A. Andres, M. Garcia-Hernandez, J.L. Martinez, Phys. Rev. B 60 (1999) 7328.
[16] Abd El-Moez A. Mohamed, Mohamed A. Mohamed, V. Vega, B. Hernando, A.M. Ahmed, RSC Adv. 6 (2016) 77284.
[17] N.F. Mott, E.A. Davis, Electronic Processes in Noncrystalline Materials, Oxford University Press, New York, 1979.
[18] M. Viret, L. Ranno, J.M.D. Coey, Phys. Rev. B 55 (1997) 8067.
[19] Z. Sheng, Y. Sun, X. Zhu, W. Song, P. Yan, J. Phys. D: Appl. Phys. 40 (2007) 3300.
[20] X.J. Liua, Z.Q. Lia, A. Yu, M.L. Liu, W.R. Li, B.L. Li, P. Wu, H.L. Bai, E.Y. Jiang, J. Magn. Magn. Mater. 313 (2007) 360.
[21] A. Dutta, N. Gayathri, R. Ranganathan, Phys. Rev. B 68 (2003) 054432.
[22] A. Asamitsu, Y. Moritomo, Y. Tokura, Phy. Rev. B 53 (1996) R2952.
[23] W. Koshibae, K. Tsutsui, S. Maekawa, Phys. Rev. B 62 (2000) 6869e6872.